RECENT RESULTS ABOUT FAN NOISE - ITS GENERATION, RADIATION AND SUPPRESSION

Charles E. Feiler
National Aeronautics and Space Administration
Lewis Research Center
Cleveland, Ohio 44135

E-1438

ABSTRACT

A review of recent developments at NASA Lewis about fan noise including its generation, radiation characteristics, and suppression by acoustic treatment is presented.

In fan noise generation, results from engine and fan experiments, using inflow control measures to suppress noise sources related to inflow distortion and turbulence, will be described. The suppression of sources related to inflow allows the experiments to focus on the fan or engine internal sources. Some of the experiments incorporated pressure sensors on the fan blades to sample the flow disturbances encountered by the blades. From these data some inferences can be drawn about the origins of the disturbances. Also, hot wire measurements of a fan rotor wake field will be presented and related to the fan's noise signature.

The radiation and the suppression of fan noise are dependent on the acoustic modes generated by the fan. It is unfortunate that these are usually not known in any detail, nor is there a really simple way to measure them. Some progress has been made in describing fan noise suppression and radiation by relating these phenomena to the mode cutoff ratio parameter. In addition to its utility in acoustic treatment design and performance prediction, cutoff ratio has been useful in developing a simple description of the radiation pattern for broadband fan noise. Some of the newer findings using the cutoff ratio parameter will be presented. Numerical methods have also been under study for sound radiation and suppression. Some comparisons of numerical theory with experimental data are presented to illustrate the potential of these methods.

INTRODUCTION

This paper reviews some of the research at the NASA Lewis Research Center on fan noise. From a theoretical viewpoint, the fan remains one of the least quantified of the noise sources in a turbofan engine. Even from this viewpoint, the physics of fan noise generation mechanisms seem to be well understood so that it is not the problem. Rather the problem seems to be that fan noise, even if consideration is restricted to tone noise at subsonic tip speed, is a consequence of several separate, simultaneous sources that depend on unsteady flows and other factors present which are all poorly quantified. Coupled with this are questions of whether the sound field will propagate (i.e., whether it is cutoff), how much sound is transmitted through either upstream or downstream blade rows, and how the sound radiates through the inlet and exhaust flow fields. All of these questions affect the far field directivity of fan noise, which is the end objective. Then, in addition to the tones, one must also consider broadband noise and, for supersonic tip speed fan operation, multiple pure tone or buzz saw noise.

Perhaps it was realization of the complexity of fan noise, as the foregoing discussion suggests, that caused Cumpsty in his 1977 review of turbomachinery noise to lament the "sharp division between theory and experiment" (ref. 1). In his view, theoretical models were simplified to the point that they had no relevance to experimental configurations, while experiments were devoted to the acquisition of overall noise with little finesse in the acquisition or the evaluation of the data. While experiment and theory are not completely reconciled today, it is the author's opinion that considerable progress has been made over the last few years since Cumpsty's review and that it is continuing.

In the present paper, all aspects of the fan noise problem will be considered - generation, duct propagation and radiation; however, the major emphasis will be on fan noise generation. The various topics will be presented in the following order:

1. Simulation of flight fan noise in static tests.

2. Rod wake-rotor interaction theory for single mode propagation.

3. Rotor wake-stator noise experiments in simulated flight.

4. Duct acoustics

In recent years a significant fraction of fan noise research has been directed toward the so-called forward velocity effects problem. Flight fan noise is less than static test fan noise. The reason is that the inflow in static tests is turbulent and contains flow distortions, perhaps from rig support wakes or other sources, that are either not present or are greatly diminished in flight. Research has focussed on the development of suitable flow-straightening devices to condition the inlet flow. References 2 to 14 contain a large fraction of this work.

Within NASA, the forward velocity effects program utilized a Pratt and Whitney of Canada JT15D turbofan engine and fan stage that were statically tested at NASA Lewis and flight tested at NASA Langley. The reconciliation of static and flight fan noise requires not only obtaining static data that duplicates flight data, but also the correct application of other factors associated with flight such as convective amplification. The NASA program will provide information about these related flight effects on fan noise when it is completed. Preliminary results from this program based on a workshop held at NASA Langley in January, 1982 will be published as a NASA Conference Publication (ref. 15). In this paper results from the static test research will primarily be discussed.

In an effort to relate experiment and theory more closely, a unique and reasonably controlled experiment was performed with the JT15D engine utilizing rods just upstream from the fan to create the noise. An inflow control device was used in this experiment to suppress the noise sources related to inflow disturbances, thus emphasizing the rod wake source. The results from this experiment and their comparison with generation theory reported in reference 16 will be described. The theory development can be found in reference 17. This significant experiment has also found important use in suppressor and radiation theory validation, as will be seen.

In a similar vein, the rotor wakes and noise from a fan stage have been measured as a function of axial spacing. This experiment is unique because of the clean flow forward velocity environment (9 by 15 Foot Anechoic Wind Tunnel) in which it was performed. The rotor wakes were measured at several radial positions. This data will be available for use in noise generation theory. Similarly, two stator sets were tested to evaluate the effects of stator number and chord. At present the comparison of these data with the theoretical model has not been completed but a sample of the results from references 18 and 19 will be presented.

Other fan noise research is concerned with duct acoustics the propagation and attenuation of sound in acoustically treated ducts, and its radiation to the far field. An understanding of duct acoustics and radiation are essential in the fan noise problem. The usual in-duct description of fan noise is in terms of duct modes. The number of modes that can propagate in a duct is approximately proportional to the square of the product of sound frequency and duct diameter (ref. 20). At the frequency of fan tones the number of modes that can propagate is quite large. In static fan-testing without flow conditioning, it appears that all of the possible modes are present (ref. 21). This may also be the case for broadband noise; however, in flight or statically with a flow straightener, the number of modes at the fan tones may be very limited. In this case the sound is due to interaction between blade rows such as rotor wake-stator interaction, and the modes generated are determined by the numbers of blades and vanes in the blade rows, as described by the Tyler-Sofrin cutoff theory (ref. 22).

A considerable simplification in handling the modes, especially when a large number is present, has resulted from the recognition that the pertinent phenomena concerning mode behavior (i.e., propagation, attenuation, optimum impedance, and radiation) are all correlated by the single mode-related parameter, cutoff ratio (refs. 21 to 27). All modes having similar values of cutoff ratio behave alike. Some of these important duct acoustics results will be included in this review.

As in other fields, there has been a significant effort to treat duct acoustics and sound radiation problems using numerical techniques. This work has been reviewed recently by Baumeister who has pioneered this field (refs. 28 and 29). Several results using this approach will be presented to illustrate the power of the technique.

SIMULATION OF FLIGHT FAN NOISE IN STATIC TESTS

As outlined in the Introduction, this research is concerned with the development of a flow straightener to be installed on an engine or fan inlet to minimize turbulence and distortions present in the inlet flow, which interact with the rotor blades to generate noise, mostly at the fan fundamental tone. Inflow control devices have all been constructed from honeycomb, often in conjunction with screens or perforated plates. In addition to smoothing the inflow, the stucture is required to allow the sound field to propagate unaltered in level and directivity.

Inflow Control Design

There was not very much concrete information to guide a design of these devices. The problem was thought to be due mostly to the ingestion of atmos-

pheric turbulence and based on the results of Loehrke and Nagib (ref. 30), screens were introduced downstream of the honeycomb. Most of the design choices seem to have been based on general knowledge and intuitive reasoning. Thus the honeycomb cells were a igned with potential flow streamlines and open area ratios of screens and perforated plates were chosen to keep pressure drops small. Honeycomb cell length/diameter ratios ranged from about two to eight. Structure size ranged from equal the fan diameter (in-duct placement) to about four times the fan diameter.

The construction method and features also had to be established. Concerns included the thickness of support ribs, the presence of corners formed by the junction of flat panels, and the achieving of a disturbance-free attachment of the structure to the nacelle. The sketches of figure 1 illustrate the three sizes of inflow control structure experimentally studied at the Lewis Research Center, along with some pertinent construction details and dimensions. The photographs in figure 2 show the devices installed on the JT15D engine at the Lewis outdoor test stand and on the JT15D fan in the Lewis anechoic chamber.

Experimental Evaluation Criteria

The effectiveness of these inflow control structures has been experimentally determined with a JT15D engine and fan stage using far-field directivity as the primary indicator. To help in the diagnosis, pressure transducers were flush mounted on the fan blades at several spanwise and chordwise locations, as shown in figure 3. The unsteady pressures sensed by these transducers were in response to velocity perturbations encountered by the blades. The velocity perturbations could arise from inlet turbulence and flow distortions, from the potential field of downstream stators or struts, and also from sound waves. These all appear as unsteady disturbances to the rotating fan.

Finally, an experiment was performed with each inflow control device to determine whether it introduced a sound transmission loss. The experiment involved the introduction of an array of 41 equally spaced rods just upstream of the fan face, as shown in figure 4. The wakes from these rods constitute a sound source that dominates all other sources and is unaffected by the presence of the inflow control structure. Thus, if the inflow control structure caused a transmission loss, it could be detected by comparing far field directivity patterns with and without the structure in place.

Experimental Observations and Interpretations

Data from the JT15D engine with and without inflow control device 1 will be compared in terms of each of these indicators: (a) far-field sound; (b) blade pressures; and (c) rod generated sound (ref. 12). The data are all at a fan speed of 10,500 rpm corresponding to a tip relative Mach number of 0.917.

Far-field sound. - Figure 5 compares narrowband spectra measured in the far field at 40° from the inlet. By comparing figures 5(a) and (b), it can be seen that the broadband noise was not affected by the inflow control device but the tones were generally reduced, the fundamental by about 10 dB and the second harmonic by about 5 dB. Interestingly, the third harmonic showed an increase of about 2 dB. The reduction of 10 dB is evidence that inflow turbulence and distortions clearly dominate the sources of the fan fundamental

tone. On the other hand, the lack of change in broadband level indicates that this noise is not related to inflow turbulence or distortions.

Figure 6 compares the directivities of the narrowband fan fundamental tone and the broadband level at the fundamental tone frequency with and without the inflow control device. Again it can be seen that the inflow control device had no effect on the broadband noise at any angle, while the tone was reduced by a larger amount forward of 40° than aft. The tone directivity with the inflow control device installed had a more lobular shape than without it. As will be shown later, this shape is largely due to a single sound mode, associated with an interaction between the fan rotor, and the six engine internal support struts downstream of the fan stators. This internal source limits the amount that the fan fundamental tone can be reduced in the JT15D engine.

Blade pressures. - Figure 7 compares spectra from a blade-mounted pressure transducer with and without the inflow control device. The tones in these spectra occur at multiples of the shaft rotational frequency and, as the middle abscissa scale suggests, these are interpreted as the circumferential mode orders q of the inflow distortion. The lower scale gives the circumferential acoustic mode number m corresponding to the interaction between any harmonic distortion q and the 28 blades B of the JT15 fan. In general, $m = B - q$. In order to propagate in the duct, an acoustic mode must spin at a rate described by the Tyler-Sofrin cut-off theory (ref. 22). For the fan speed of figure 7, cut-off occurs for mode numbers over 23 or less than 23 corresponding to distortion harmonics less than five and over 51.

Without inflow control (fig. 7(a)), the spectrum consists of peaks at every shaft harmonic in the frequency range of the spectrum. Based on the preceding interpretation, this means that all the modes that can propagate should be present in the sound field. Unfortunately the blade pressure data do not suggest what the mode amplitudes are.

In contrast, the spectrum with the inflow control device (fig. 7(b)) is reduced to peaks at distortion harmonics q of 1, 2, 5, 6, and 12. The conclusion is that most of the peaks in the baseline spectrum were the result of turbulence or other distortions entering the inlet that the inflow control device eliminated. The five or so peaks remaining with inflow control are presumably due to spatially fixed disturbances such as the six structural struts just downstream of the fan stators.

That these are spatially fixed disturbances can be reasonably demonstrated by examining the signal-enhanced wave form and its spectrum. This wave form averaged over 200 rotor revolutions (fig. 8(a)) and shows the presence of fixed patterns of 1, 6, and 66 peaks per revolution. The spectrum of this wave form (fig. 8(b)) confirms the presence of peaks phase-locked with the rotor at $q = 1$, 2, 5, 6, and 12. The peak at $q = 66$ appears in spectra carried out to its frequency. It is due to the 66 stators in the JT15D fan. Of the peaks present, those at $q = 6$ and 12 yield propagating acoustic modes that are presumably the primary cause of the residual fan fundamental tone, observed with the inflow control device. The peak at $q = 6$ is probably related to the six engine support struts mentioned earlier. According to the previous discussion, these should generate an acoustic mode, $m = 22$, with 22 circumferential lobes. To evaluate this conclusion, two pressure sensors were flush-mounted within the JT1D inlet at the same axial plane but 1/44 of the circumference apart. If there were a 22 lobe pattern, these sensors should

sense the same signal with a 180° phase difference. The measured traces, shown in figure 9, show this result precisely which seems to confirm the presence of the 22 lobe acoustic mode. These distortions are also the source of a fundamental tone in flight, if they are indeed the consequence of some engine-related internal flow disturbance. The data, however, do not reveal whether the sources are within or external to the engine. That has to come from other evidence or reasoning. For example, the once per revolution source (q = 1) may be due to the presence of a ground plane, whereas q = 6 appears to come from the engine struts.

Rod-generated sound. - The 41 rods constitute a distortion having a harmonic number of 41 and, from the preceding discussion, should generate a 13-lobe acoustic mode whose strength is independent of inflow turbulence or distortions. It is this sound field that was used to determine whether the inflow control device alters the sound transmission. Figure 10 compares the far-field directivities of the rod-generated tone with and without the inflow control device. It also shows the tone directivity without rods or inflow control from figure 6. The strong contribution of the rod source can be seen in the range from 30 to 60°. It can also be seen that the directivity was hardly altered by installation of the inflow control device, hence, the conclusion that it does not affect sound transmission. The same conclusion can be drawn from comparing the broadband levels at the tone frequency, as also shown in figure 10.

Summary and Limited Comparisons with Flight Data

It has been demonstrated that an inflow control device does not alter the sound transmission and can reduce or eliminate the noise caused by inflow turbulence or distortions by smoothing the inlet flow. The use of inflow control has allowed static experiments to focus on the internal engine and fan design-related fan noise sources. Already, these experiments, even those intended only to validate and demonstrate inflow control devices, have provided improved understanding of fan noise. For example, it appears that inflow turbulence is not the dominant cause of fan broadband noise, a new conclusion. As another example, with inflow control, the rod data have served as a reasonably defined controlled noise source that has been useful in validating source noise models, radiation or directivity models, and acoustic treatment design procedure (as will be seen in subsequent sections of this paper). The experiments have also revealed that engine design features (e.g., supports) can be a source of fan noise that could have been overlooked in the past since they could not have been identified in static tests. Clearly, the inflow control device is an important success in fan and engine acoustic experimentation. Although the evaluation is not yet complete and is complicated by some significant flight effects, the preliminary comparisons, made at Langley Research Center between their JT15D flight data and Lewis static data, show that many features of the flight data are reproduced by static data obtained with inflow control (ref. 15).

Figure 11 compares flight and static spectra with ICD No. 12 from the JT15D. Except for a reduction of about 6 dB in the broadband level in flight, the spectra, including the absence of a fan fundamental tone, are quite similar. The shift in broadband level is largely due to a shift to a lower engine operating line in the flight data. Figure 12 compares the flight and static tone directivities. Again the agreement is good at angles from about 50° and aft. At angles forward of 50°, the flight data roll off faster than to the static data, possibly due to a real flight effect such as convective

amplification. In any case, we conclude that the inflow control device appears to do a reasonable job in solving the fan static testing problem.

COMPARISON OF THEORY WITH SINGLE MODE EXPERIMENT

The experiment with the 41 rods as a noise source was described earlier. The rod wakes generated a fan tone that dominated or controlled the measured noise and since the wakes from the rods are known, the experiment offered a unique opportunity for comparison with theory. The theory, developed in reference 17, is three-dimensional and treats the source as noncompact. Details of the results presented here are given in reference 16. Figure 13 compares the measured and calculated fundamental fan tone power due to the 41 rod wakes interacting with the JT15D fan. The comparison is shown as a function of fan speed and displays the individual mode powers as they begin to propagate. The agreement is excellent over the entire speed range. It is interesting that the increase in tone power is not monotonic with speed, either experimentally or theoretically. Also the modal power mix varies with speed.

These two results, if general, illustrate the difficulty of developing a universal fan noise correlation. The next elements needed in the theoretical development are to incorporate a far field directivity model and to account for the modal-scattering that may occur as the inlet duct changes geometry from annular to circular. The agreement between theory and experiment in terms of sound power provides some confidence that the aeroacoustic modeling is valid and can give useful results if the input disturbance is adequately known. A more important practical case than inflow distortion-rotor interaction is rotor wake-stator interaction, which is considered in the next section.

ROTOR WAKES AND NOISE

The experimental results were obtained in the Lewis 9 by 15 Foot Anechoic Wind Tunnel using a fan simulator (refs. 18 and 19). The installation in the tunnel is shown in figure 14. With a low tunnel velocity, the inflow into the fan is smooth enough that the noise due to this source is not a problem and the experiment can focus on rotor-stator interaction noise. In the experiments the wakes and resulting noise of a 15-bladed rotor, rotor 55, were measured as a function of rotor-stator axial spacing for two stators as shown in figure 15. The stators had vane numbers of 25 and 11 that resulted in cutoff and cuton, respectively, of the fundamental tone due to rotor-stator interaction. There were also more propagating modes at each of the higher harmonics with the 11-vane stator than with the 25-vane stator. The 11-vane stator has a larger chord than the 25-vane stator since solidity was maintained constant and, thus, the dynamic response of the 11-vane stator shoud be different from that of the other because of its lower reduced frequency (ratio of gust wavelength to stator chord).

Rotor Wakes

The wakes were measured with stationary cross film anemometers located in the stator, leading edge-plane midway between adjacent vanes as shown in figure 16. The films were alined, as shown in figure 17, to measure the streamwise and upwash velocity components at the stato. leading edge. Wake measurements were obtained at four radial immersions from near the rotor tip to vicinity of the hub. The fixed reference frame data were digitally proc-

essed and combined with the fan rotational velocity to obtain the wake profile in the rotating reference plane.

Figure 18 shows the rotor relative and upwash velocities as a function of radial position. The profiles, showing seven consecutive blades of the 15 rotor blades, represent averages from 500 rotor revolutions. These data are at a fan tip speed of 560 ft/sec, corresponding to 80 percent of design speed, and a downstream distance of 1.23 aerodynamic rotor chords. It can be seen that the wake profiles are nearly identical from blade to blade. Away from the tip the profiles are about as expected; however, near the tip a double defect appeared, probably due to the presence of a tip vortex that lies about midway between adjacent wakes. The wake defect amplitude decreased inward from the tip but then showed an increase at the location nearest the hub.

The upwash velocity component is more important to noise generation. There is a one-to-one frequency correspondence between the wake and sound harmonics. Thus, the spectral content of the wakes is of direct interest. Figure 19 shows the spectrum of the upwash wave form, shown in figure 18(b) at 30 percent of the span from the tip. At this intermediate position the spectrum levels show a regular falloff with increasing harmonic number. Figure 20 shows the levels of the first four harmonics as a function of distance downstream from the rotor. Data are shown at the 30 and 9 percent spanwise positions. At 30 percent span, the harmonic order remained constant with increasing distance and the higher harmonics appeared to decay faster than the fundamental, an expected result. On the other hand, near the tip, the second harmonic was largest and decayed slower with increasing downstream distance. Initially the third harmonic was also greater than the fundamental which, however, became larger at the farthest position. This unusual behavior at the tip must be related to the tip vortex. It is complicated not only by the wake decay that occurs, but also by the ability of the vortex to migrate radially as it moves downstream.

These wake velocity harmonic amplitudes are the necessary input parameters to a rotor-stator interaction noise theory. As these data show, the wake from a rotor can be rather complex. Their representation by a simple Gaussian profile may not be adequate in many cases and this could lead to the poor agreement between theory and experiment, discussed in the Introduction. This may also be an example of the concerns that Cumpsty alluded to.

Rotor Wake-Far Field Noise Experiment

Narrowband spectra of the inlet quadrant sound power measured for the two stator sets are shown in figure 21 at 80 percent of fan speed. With the 25-vane stator the fundamental tone amplitude was quite low because the modes due to rotor-stator interaction were cutoff; hence, the tone, not being dependent on the interaction, was weak. In contrast, the fundamental tone dominated the spectrum for the 11-vane stator. Here there was a propagating mode from interation.

The variation of inlet sound power for the first three harmonics is shown as a function of rotor-stator spacing for both stators in figure 22. In general, the levels decreased with increased spacing. The exception was the fundamental tone. For the 25-vane stator, as described, there were no propagting modes and this tone decreased only slightly with increased spacing. For the 11-vane stator, the tone decreased at first and then leveled off or increased

slightly as spacing was increased. This behavior is likely a consequence of the behavior observed for the fundamental harmonic of the tip upwash velocity, which followed the same trend.

Because tip velocities are highest, it might have been expected they would control the sound generation; however, as was discussed earlier, the behavior of the wake velocity harmonic content with downstream distance could not have been anticipated from existing wake models. These data strongly reinforce the conclusion that knowledge of the wake structure is essential for predicting the rotor-stator interaction noise from fans. At present there is an effort underway at Lewis using these data to evaluate a theoretical model; the preliminary results are encouraging. This effort will include the difficult but necessary next step of going to the far field which requires the addition of a sound radiation model.

DUCT ACOUSTICS

Duct acoustics research can be conveniently separated into analytical and numerical methods. In the following discussion, analytical results based on the cutoff ratio approach will be presented, followed by a summary of a recent numerical study. Finally several other interesting results from analytical studies will be presented.

Analytical - Cutoff Ratio Approach

The in-duct sound field generated by a fan stage is ordinarily defined in terms of spinning modes, as was discussed in the Introduction. For a circular or annular duct, two indices representing the circumferential and radial mode orders are required. Fan broadband noise and fan tones, when generated statically without inflow control, appear to consist of all the propagating modes that the duct can sustain (ref. 21). At fan tone frequencies they may number in the hundreds. In view of the large number of modes possible and in recognition of the extreme difficulty in measuring the mode content or calculating it, the theoretical behavior of modes was examined to find some simplification that would make the handling of duct-related problems more tractable. In determining the optimum impedance (resistance and reactance) for various sound modes propagating in a circular duct with sheared flow, Rice (refs. 23 and 31) observed that modes with widely differing mode indices required, for a given frequency, duct velocity and boundary layer thickness, the same optimum impedance (resistance and reactance), and had the same theoretical attenuation. The correlation parameter was mode cutoff ratio and was immediately used as the basis of a suppressor design method (ref. 32). In subsequent papers, inlet and aft sound radiation and duct termination loss were also correlated with cutoff ratio (refs. 21 and 26). These phenomena were then incorporated into the suppressor methodology to yield a prediction of far field attenuation directivity, the ultimate goal (refs. 27, 33, and 34). As a part of the method, a modal density function based on cutoff ratio was derived which allowed the mode distribution to be easily biased toward or away from cutoff (ref. 20). In addition to describing attenuation directivity, the method also describes the attenuation of the suppressor at off-design cutoff ratios and off-design sound frequencies. Finally, to understand the physics of duct acoustics better, it was shown that cutoff ratio is related to mode propagation angle, a somewhat more basic parameter that also could have been used as the basis of the method (refs. 24 and 25).

Suppressor properties and cutoff ratio. - A sampling of these results follows, starting with the correlation of optimum resistance with cutoff ratio, showing boundary layer thickness as a parameter (ϵ = boundary layer thickness/duct radius) (fig. 23). The correlation equation (curves) agrees with the exact calculation (data points) very well, and all the modes lie on a single line for a given boundary layer thickness. The effect of boundary layer thickness is small for modes near cutoff but is large for modes that have high cutoff ratio. In the latter case, the mode propagation is mostly axial and the wave is refracted by the boundary layer. At cutoff the mode propagation direction is transverse and no refraction occurs.

Exact calculations of the optimum reactance are shown in figure 24 as a function of mode-cutoff ratio. Again, cutoff ratio correlates the data onto a single line for each value of boundary layer thickness, which is very well described by the correlating equation. The dependence of optimum reactance on boundary layer thickness shows trends similar to those of resistance for the same reason.

Finally, figure 25 shows the maximum sound power attenuation (that at the optimum inpedance) as a function of cutoff ratio. The calculations are for a matrix of modes with lobes 1, 7, and 10, each with radial orders of 1, 2, 5, and 10. With the exception of radial orders 1 and 2 at a lobe of 1, the data are moderately well collapsed by cutoff ratio. For moderate to high values of cutoff ratio, the attenuation varies inversely with cutoff ratio. The high attenuations at low value of cutoff ratio occur because these modes propagate transversely and are easier to absorb than those at high cutoff ratio, whose propagation is more axial.

These correlations with cutoff ratio clearly reveal the utility of cutoff ratio in suppressor design. In the next section, its utility in sound ratiation will be discussed.

Radiation and cutoff ratio. - Rice has also derived very useful approximations based on cutoff ratio for the directivity of single modes and multimodal distributions with equal power per mode. Both inlet and exhaust duct radiation have been treated, including the effect of the shear layer for exhaust radiation. Since most of the energy in a single mode is carried by the principal lobe, it becomes important to predict the directivity angle where it peaks.

Figure 26 shows the angle of principal lobe peak as a function of cutoff ratio for the case of no external flow (static testing). The effect of duct Mach number is also shown. Increasing the duct Mach number causes both the inlet-and exhaust-radiated sound to radiate to more forward angles. In fact, aft sound modes approaching cutoff are radiated well into the inlet quadrant. At 90°, the overhead position during flyover, the aft radiated sound occurs in modes well above cutoff. Based on the earlier discussion of maximum attenuation, this noise would be difficult to suppress. In contrast, the inlet noise at 90° is due to modes very near or at cutoff, these being very easy to suppress.

The approximate exhaust radiation model based on cutoff ratio can be checked by comparison with exact solutions obtained by the Wiener-Hopf method. Figure 27 compares the approximate and exact methods for a single mode. The agreement between the two methods is very good. Mode-lobe patterns are reproduced as is the angle marking the zone of silence. In the exact solu-

tion, some sound reaches angles within this zone but the approximate method does not permit sound to enter the region because of its geometric acoustic characteristics. The approximate method thus appears to contain all the essential features of aft duct sound radiation, including the effects of duct Mach number and the external jet shear layer.

In the inlet there is no shear layer to contend with but the effect of duct Mach number predicted by the approximate method is of some concern. There is no exact solution for inlet-radiated sound for the static test case, with no external flow but a duct Mach number. The Wiener-Hopf method only gives results for two cases: uniform flow everywhere and no flow. An attempt was made to validate the inlet radiation, using data for the rod-generated tone from the JT15D engine that was described earlier (ref. 35). This comparison is shown in figure 28. In this figure, the lobe due to the rod wake-fan interaction is compared with the approximate method result and the Wiener-Hopf solution for flow everywhere. The data show the expected forward translation of the mode as engine speed was increased. This is due to the increase in mode cutoff ratio and is shown by both models. At the two lower speeds, the approximate model, duct flow alone, appears to match the data better; however, at the two higher speeds, the exact solution based on uniform flow everywhere seems to provide the better match. The results, therefore, are not wholly conclusive and additional work will be needed to resolve this issue. The numerical method of the following section while it cannot handle these higher duct Mach numbers at present, will ultimately be capable of solving this problem

Directivity models for broadband sound and for other multimodal cases such as for tones, due to inflow distortion or turbulence, are of some importance. A case that has received some attention, because it appears to fit these two situation, is a multimodal model with all the possible propagating modes present with equal sound powers. The model, described in reference 21 for inlets, is based on cutoff ratio. The model yields a very simple expression, $P^2 = 2 \cos \Psi$, where P^2 is the mean square sound pressure and Ψ is the far-field directivity angle. This equation is compared in figure 29 with the exact result obtained by summing the levels of all the propagating modes. In this case there were over 1000 modes. The agreement is excellent.

A similar comparison is made in figure 30 for exhaust radiated noise, as developed in reference 26. The model yields the expression

$$P^2 = 2\left(1 - M_D^2\right)\left[M_D + \left(1 - M_D^2\right)\cos \Psi\right]$$

where M_D is the duct Mach number and the other symbols are as previously defined. This equation is compared, in figure 30, with the exact result obtained by summing over all the propagating modes calculated by the Wiener-Hopf method. For the conditions shown, there were 101 propagating modes. The agreement between the approximate and exact multimodal models is very good, except at the forward-or inlet-quadrant angles where the directivity by the approximate method falls off more rapidly than it does by the exact method. The approximate method describes the angle for the zone of silence correctly but, again, does not permit any sound within this zone.

Once again these results illustrate the utility of cutoff ratio as a tool for describing sound propagation and radiation, and for understanding the phenomena that occur.

Numerical Methods

The potential for handling variable area inlet or exhaust ducts with their complex flow gradients provides motivation for solving duct acoustics propagation problems numerically. Soft-walls as well as radiation to the far-field can be handled. As a special case, the sonic or near-sonic inlet was of interest. Numerical analysts have explored finite difference and finite element methods and steady state and transient formulations of the problem. Most of the phenomena of interest are described by linear theory. The important exception is the near-sonic or sonic inlet where nonlinear theory is apparently required.

The experimental data from the JT15D engine with rods (already mentioned several times) have been compared with results of numerical calculations in reference 36. In the experiment, the far-field directivities of the rod-generated fan tone were measured with a hard-walled inlet and an acoustically treated inlet. The acoustic liner was designed for the particular mode (13,0), using the cutoff ratio procedure mentioned earlier. The numerical method coupled a finite element solution in the duct, capable of handling acoustically treated walls as well as hard walls, with an integral solution in the far field.

Figure 31 shows the inlet with the acoustic treatment and the tone-generating rods. Of interest is the very large radius of the inlet lip employed in these static tests. Figure 32 compares the experimental and theoretical results. The numerical method agrees with the data very well. The figure also shows a calculated directivity curve according to the Wiener-Hopf method discussed earlier. The agreement between this calculation and the data is very good from the peak angle forward. Aft of the peak the Wiener-Hopf method greatly overpredicts the data. This result is probably due to the inability of the Wiener-Hopf method to account for the very thick-lipped inlet, since this method can only handle a very thin-inlet lip. The results point to a considerable acoustic shielding of the aft angles by the inlet lip. The inlet Mach number in the experiment was too low to have had a significant effect.

Figure 33 shows the measured and predicted attenuations as a function of liner resistance. It can be seen that the numerical method agrees very well with the data. At this engine speed, the rod wakes generate a single propagating mode that was input into the calculation. Since the sound field does consist of a single mode, the attenution directivity should not be a function of angle. The data, shown for four angles, confirm this conclusion within a scatter of about ± 1 dB.

The potential and versatility of the numerical methods are clearly demonstrated by these comparisons. The chief limitation of the method, at present, is the lack of storage capacity in the computer to handle propagating modes (well above cutoff) with short axial wavelengths. The convective effect of increasing inlet Mach number serves to shorten wavelength further and accentuate the limitation. These facts limit the method to lower sound frequencies and duct Mach numbers.

Other Analytical Development

There are other results that will only be briefly discussed. In the area of duct propagation, Cho (refs. 37 and 38) showed that there is no mode-scattering in traveling through a variable area duct, if the flow gradients are not too large (as is probably true for most practical cases). Cho (ref. 39) also developed a theory describing the refraction of a sound ray by the flow near the inlet lip, which he modeled as a vortex.

In suppressors, a theory for extended reaction (bulk absorber) liners is being developed that will permit the proper design of extended reaction liners (ref. 40). Already the theory explains the increased bandwidth absorption by these liners. The grazing flow impedance of Helmholtz resonators (perforated plate over honeycomb) has also been successfully modeled (ref. 41).

CONCLUDING REMARKS

The results presented in this paper, largely from activities at the Lewis Research Center, have been selected to illustrate the significant progress in all aspects of fan noise. Whereas earlier work without inflow control did not display much sensitivity to fan design for the large rotor-stator spacings employed in high bypass engine fan stages, later research with inflow control, by flow straighteners or actual forward velocity, has revealed a great deal of sensitivity to design. Many of the theoretical results predicted such as mode cutoff, radiation patterns, and suppressor performance are observed both qualitatively and quantitatively with inflow control.

Fan noise generation models, now predicting mode amplitudes and phases, are currently being modified to include duct propagation and radiation so that far-field directivity patterns can be predicted. Suppressor performance is also being predicted in terms of far-field directivity patterns. The numerical approach to propagation and radiation, if it can be extended to higher frequency and duct Mach number, will contribute notably to these capabilities.

It is the author's opinion that, although the problems are not fully solved, there has been considerable advancement in all aspects of fan noise.

REFERENCES

1. Cumpsty, N. A.: A Critical Review of Turbomachinery Noise. J. Fluids Eng., Vol. 99, no. 2, June 1977, pp. 278-293.

2. Feiler, C. E.; and Groeneweg, J. F.: Summary of Forward Velocity Effects on Fan Noise. AIAA paper 77-1319, Oct. 1977. (NASA TM-73722.)

3. Lowrie, B. W.; and Newby, D. R.: The Design and Calibration of a Distortion-Reducing Screen for Fan Noise Testing. AIAA paper 77-1323, Oct. 1977.

4. Cocking, B. L.; and Ginder, R. B.: The Effect of an Inlet Flow Conditioner on Fan Distortion Tones. AIAA paper 77-1324, Oct. 1977.

5. Blankenship, G. L.: Effect of Forward Motion on Turbomachinery Noise. AIAA paper 77-1346, Oct. 1977.

6. Jones W. L.; McArdle, J. G.; and Homyak, L.: Evaluation of Two Inflow Control Devices for Flight Simulation of Fan Noise Using a JT15D Engine. AIAA paper 79-0654, Mar. 1979. (NASA TM-79072.)

7. Ho, P. Y.; and Smith, E. B.: An Inflow Turbulence Reduction Structure for Scale Model Fan Testing. AIAA paper 79-0655, Mar. 1979.

8. Kantola, R. A.; and Warren, R. E.: Reduction of Rotor-Turbulence Interaction Noise in Static Fan Noise Testing. AIAA paper 79-0656, Mar 1979.

9. Ginder, R. B.; Kenison, R. C.; and Smith, A. D.: Considerations for the Design of Inlet Flow Conditioners for Static Fan Noise Testing. AIAA paper 79-0657, Mar. 1979.

10. Rogers, D. F.; and Ganz, U. W.: Aerodynamic Assessment of Methods to Simulate Flight Inflow Characteristics during Static Engine Testing. AIAA paper 80-1023, Mar. 1980.

11. Atvars, Y.; and Rogers, D. F.: The Development of Inflow Control Devices for Improved Simulation of Flight Noise Levels during Static Testing of a HBPR Turbofan Engine. AIAA paper 80-1024, June 1980.

12. McArdle, J. G.; etal.: Comparison of Several Inflow Control Devices for Flight Simulation of Fan Tone Noise using a JT15D-1 Engine. AIAA paper 80-1025, June, 1980. (NASA TM-81505.)

13. Perracchio, A. A.: Assessment of In-Flow Control Structure Effectiveness and Design System Development. AIAA paper 81-2048, Oct. 1981.

14. McArdle, J. G.; Homyak, L.; and Chrulski, D. D.: Turbomachinery Noise Studies of the AIResearch QCGAT Engine with Inflow Control. AIAA paper 81-2049, Oct. 1981.

15. Chestnutt, D., ed.: Simulation of Fan Noise in Flight and Flight Effects. NASA CP 2242, Sept., 1982.

16. Kobayashi, H.; and Groeneweg, J. F.: Effects of Inflow Distortion Profiles on Fan Tone Noise. AIAA J., Vol. 18, no. 8, Aug., 1980, p. 899-906.

17. Kobayahsi, H.: Three-Dimensional Effects on Pure Tone Fan Noise Due to Inflow Distortion. AIAA paper 78-1120, July 1978. (NASA TM-78885.)

18. Shaw, L. M.; and Balombin, J. R.: Rotor Wake Characteristics Relevant to Rotor-Stator Interaction Noise Generation. AIAA paper 81-2031, Oct. 1981. (NASA TM-82703.)

19. Woodward, R. P.; and Glaser, F. W.: Effects of Blade-Vane Ratio and Rotor-Stator Spacing on Fan Noise with Forward Velocity. AIAA paper 81-2032, Oct. 1981. (NASA TM-82690.)

20. Rice, E. J.: Modal Density Function and Number of Propagating Modes in Ducts. Presented at the 92nd Accoustical Society of America Meeting, (San Diego, CA), Nov. 16-19, 1976. (NASA TM-73539.)

21. Rice, E. J.: Multimodal Far-Field Acoustic Radiation Pattern Using Mode Cutoff Ratio. AIAA J., Vol. 16, no. 9, Sept. 1978, pp. 906-911. (NASA TM-73721.)

22. Tyler, J. M.; and Sofrin, T. G.: Axial Flow Compressor Noise Studies. SAE Trans., Vol. 70, 1962, pp. 309-332.

23. Rice, E. J.: Optimum Wall Impedance for Spinning Modes-A Correlation With Cutoff Ratio. AIAA paper 78-193, Jan. 1978. (NASA TM-73862).

24. Rice, E. J.; Heidmann, M. F.; and Sofrin, T. G.: Modal Propagation Angles in a Cylindrical Duct with Flow and their Relation to Sound Radiation. AIAA paper 79-0183, Jan. 1979. (NASA TM-79030.)

25. Rice, E. J.: Modal Propagation Angles in Ducts with Soft Walls and their Connection with Suppressor Performance. AIAA paper 79-0624, Mar. 1979. (NASA TM-79081.)

26. Rice, E. J.; and Saule, A. V.: Farfield Radiation of Aft Turbofan Noise. Presented at the 99th Meeting of the Acoustical Society of America, (Atlanta, GA.), Apr. 21-25, 1980. (NASA TM-81506.)

27. Rice, E. J.; and Sawdy, D. J.: A Theoretical Approach to Sound Propagation and Radiation for Ducts with Suppressors. Presented at the 101st Meeting of the American Acoustical Society, (Ottawa, Ontario), May 18-22, 1981. (NASA TM-82612.)

28. Baumeister, K. J.: Numerical Techniques in Linear Duct Acoustics - A Status Report. J. Eng. Ind., Vol. 103, Aug. 1981, pp. 271-281.

29. Baumeister, K. J.: Numerical Techniques in Linear Duct Acoustics - 1980-81 Update. Presented at the ASME 102nd Winter Annual Meeting, (Washington, D.C.). Nov. 15-20, 1981. (NASA TM 82730.)

30. Loehrke, R. I.; and Nagib, H. M.: Control of Free Stream Turbulence by Means of Honeycombs: A Balance Between Suppression and Generation. Fluids Eng., Vol. 98, no. 3, Sept., 1976, pp. 342-353.

31. Rice, E. J.: Acoustic Liner Optimum Impedance for Spinning Modes with Mode Cutoff Ratio as the Design Criterion. AIAA paper 76-516, July 1976, (NASA TM X-73411.)

32. Rice, E. J.: Inlet Noise Suppressor Design Method Based Upon the Distribution of Acoustic Power with Mode Cutoff Ratio. Advances in Engineering Science. NASA CP-2001, Nov. 1976, pp. 883-894.

33. Rice, E. J.; and Heidelberg, L. J.; Comparison of Inlet Suppressor Data with Approximate Theory Based on Cutoff Ratio. J. Aircraft, vol. 18, no. 10, Oct. 1981, pp. 810-817.

34. Heidelberg, L. J.; Rice, E. J.; and Homyak, L.: Experimental Evaluation of a Spinning-Mode Acoustic-Treatment Design Concept for Aircraft Inlets. NASA TP-1613, 1980.

35. Heidmann, M. F.; Saule, A. V.; and McArdle, J. G.: Analysis of Radiation Patterns of Interaction Tones Generated by Inlet Rods in the JT15D Engine. AIAA Paper 79-0581, Mar. 1979, (NASA TM-79074.)

36. Baumeister, K. J.; and Horowitz, S. J.: Finite Element-Integral Simulation of Static and Flight Fan Noise Radiation from the JT15D Turbofan Engine. NASA TM-82936, Aug. 1982.

37. Cho, Y. C.; and Ingard, K. U.: Closed Form Solution of Mode Propagation in a Nonuniform Circular Duct. AIAA J., Vol. 20, No. 1, Jan. 1982, pp. 39-44.

38. Cho, Y. C.; and Ingard, K. U.: Mode Propagation in Nonuniform Circular Ducts with Potential Flow. AIAA Paper 82-0122, Jan. 1982. (NASA TM-82776.)

39. Cho, Y. C.; and Rice, E. J.: High-Frequency Sound Propagtion in a Spatially Varying Mean Flow. Paper presented at the 100th Meeting of the Acoustical Society of American, (Los Angeles, CA.), Nov., 1980. (NASA TM 81751).

40. Hersh, A. S.; Walker, B.; and Dong, S. B.: Analytical and Experimental Investigation of the Propagation and Attenuation of Sound in Extended Reaction Liners. AIAA Paper 81-2014, Oct. 1981.

41. Hersh, A. S.; and Walker, B.: Fluid Mechanics Model of the Helmholtz Resonator. NASA CR-2904, Sept. 1977.

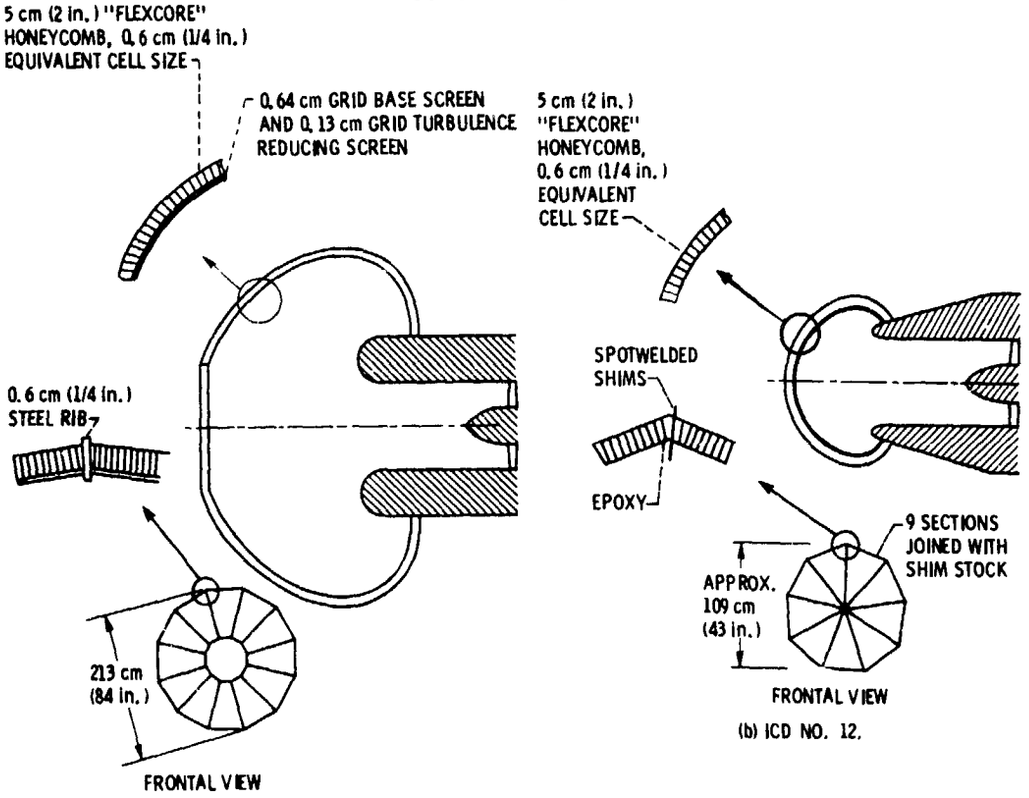

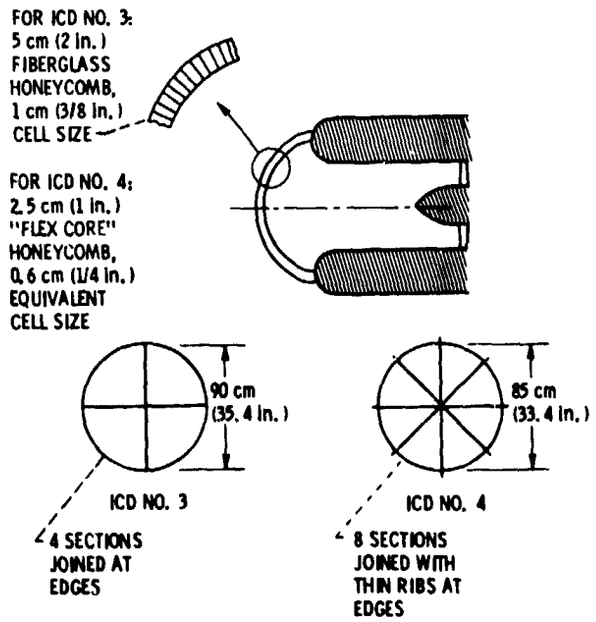

Figure 1. - Inflow control devices (ICD) tested at the Lewis Research Center.

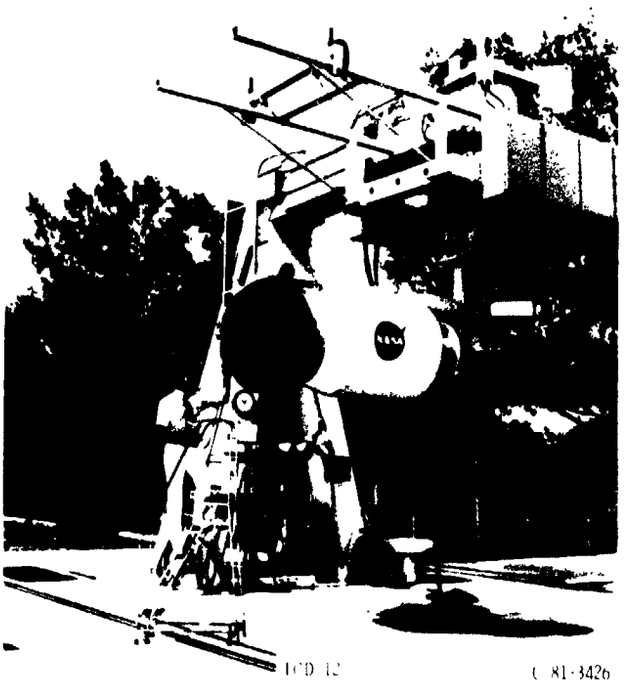

(a) INFLOW CONTROL DEVICE NO. 12 MOUNTED ON JT15D.

Figure 2. - Engine inlet at the Lewis outdoor engine test stand.

(b) INFLOW CONTROL DEVICE NO. 1 MOUNTED ON JT15D, FAN INLET IN THE LEWIS ANECHOIC CHAMBER.

Figure 2. - Concluded.

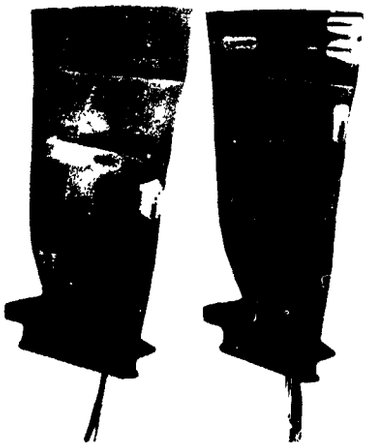

(a) INSTRUMENTED BLADES.

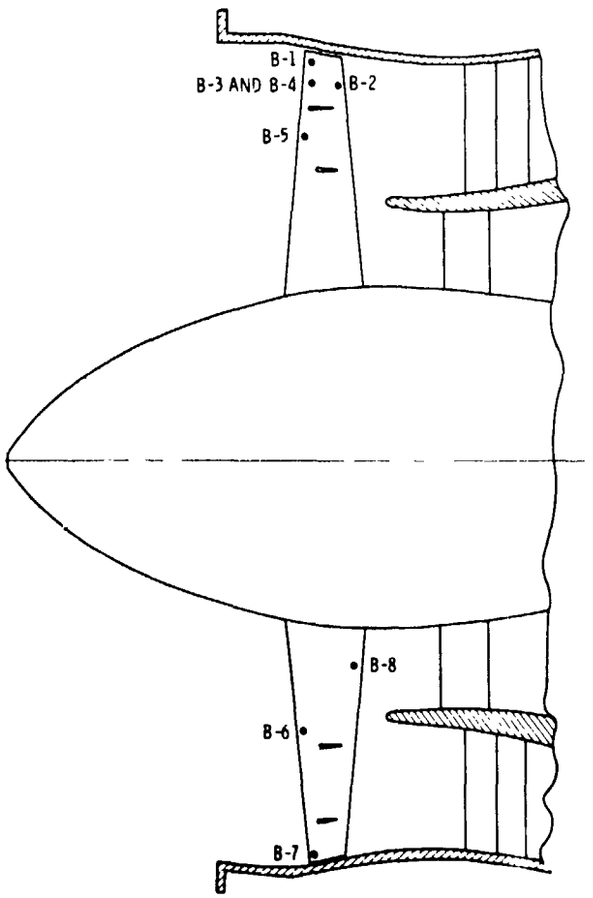

TRANSDUCER	DISTANCE FROM WALL, cm (in.)	SURFACE MEASURED	MOUNTING STYLE
B-1	0.64 (0.25)	PRESSURE	SURFACE
B-2	1.90 (0.75)		
B-3			
B-4		SUCTION	
B-5	5.08 (2.00)	PRESSURE	
B-6	8.89 (3.50)		
B-7	0.64 (0.25)		HOLE
B-8	12.7 (5.00)		SURFACE

(b) TRANSDUCER LOCATIONS.

Figure 3. - Blade mounted pressure transducers.

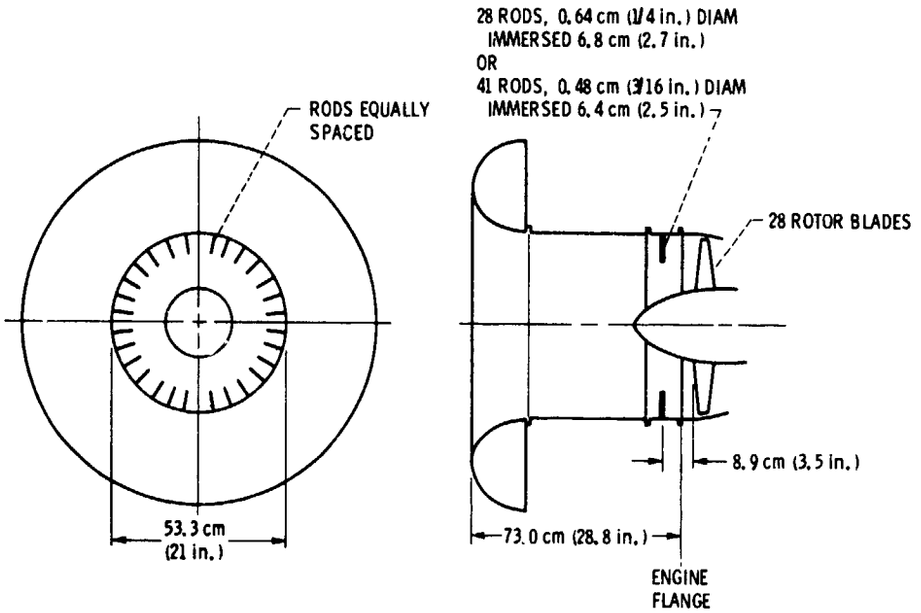

Figure 4. - Schematic diagram of rod installation.

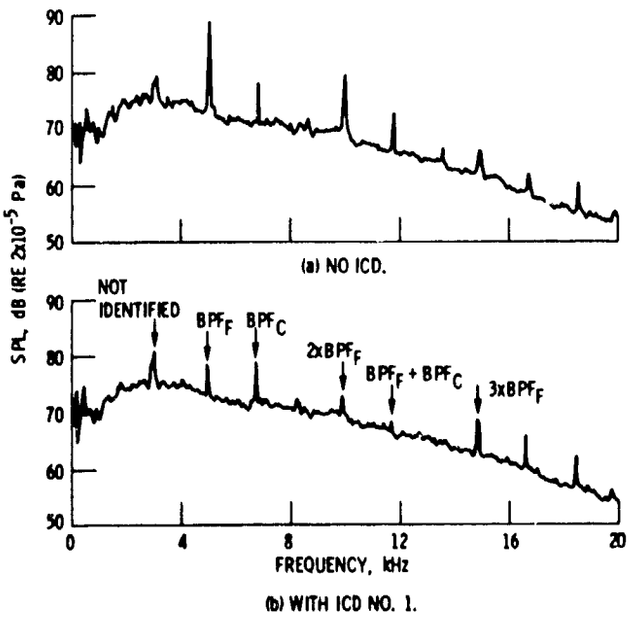

Figure 5. - Narrow-band spectra for ground microphone at 27.4 m (90 ft), 40° from engine inlet axis; corrected fan speed 10 500 rpm; analyzer bandwidth 25 Hz.

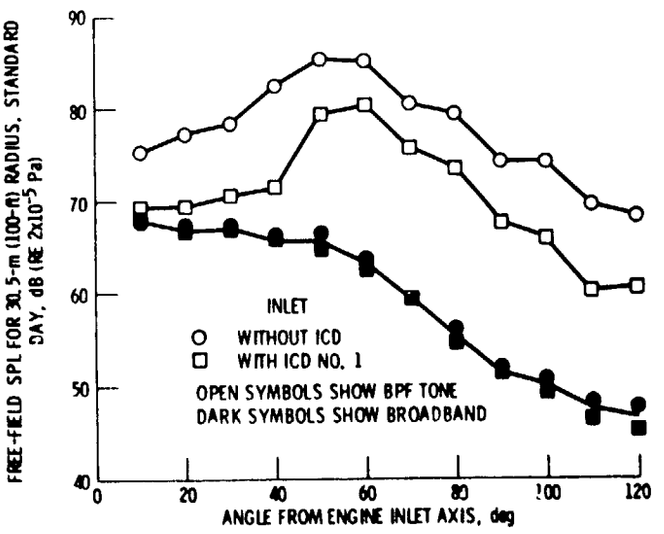

Figure 6. - Far-field directivity patterns at 10 500 rpm fan speed. Analyzer bandwidth 25 Hz.

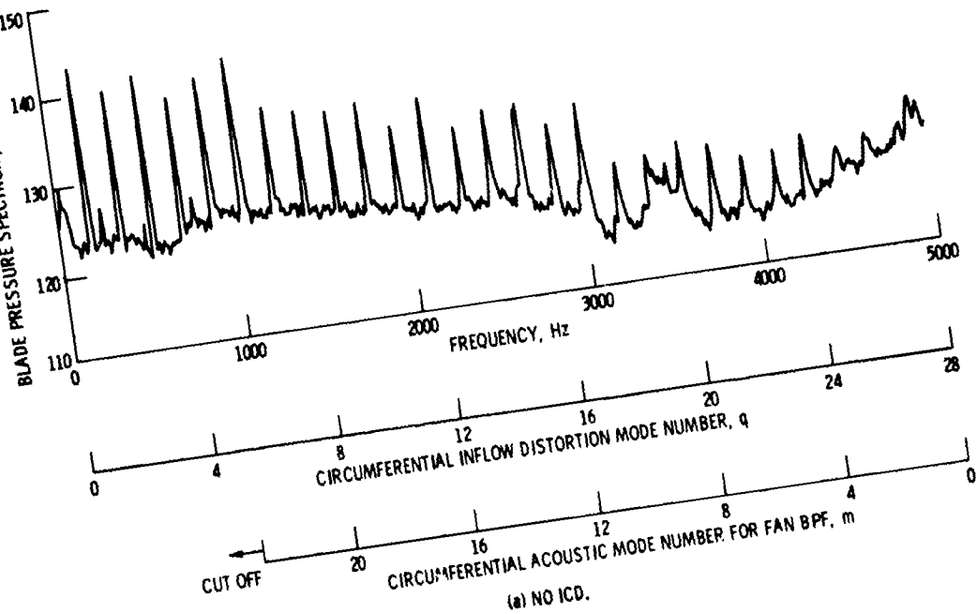

(a) NO ICD.

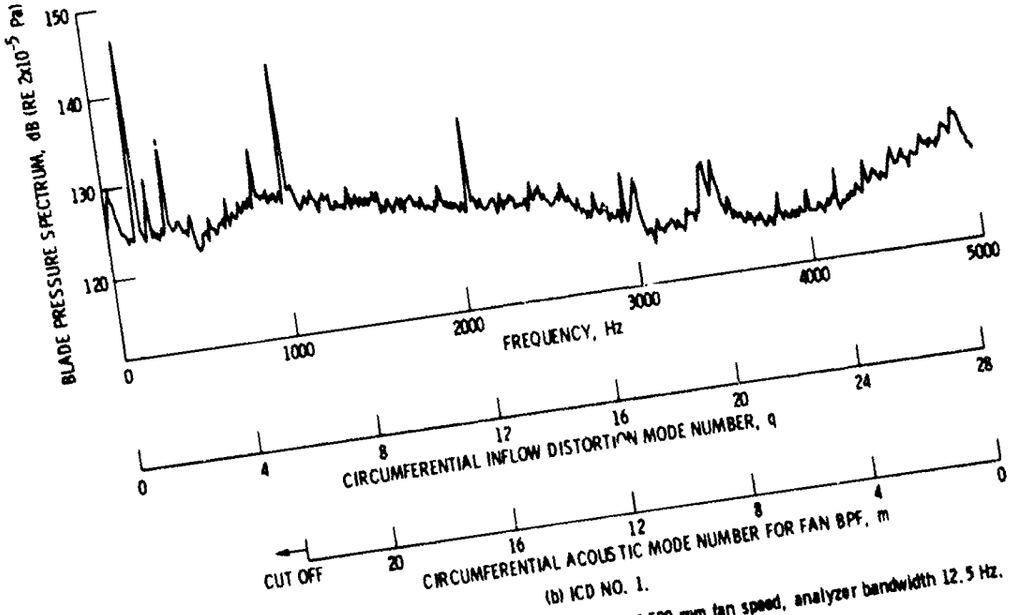

(b) ICD NO. 1.

Figure 7. - Blade pressure spectrum for transducer B-3; 10 500 rpm fan speed, analyzer bandwidth 12.5 Hz.

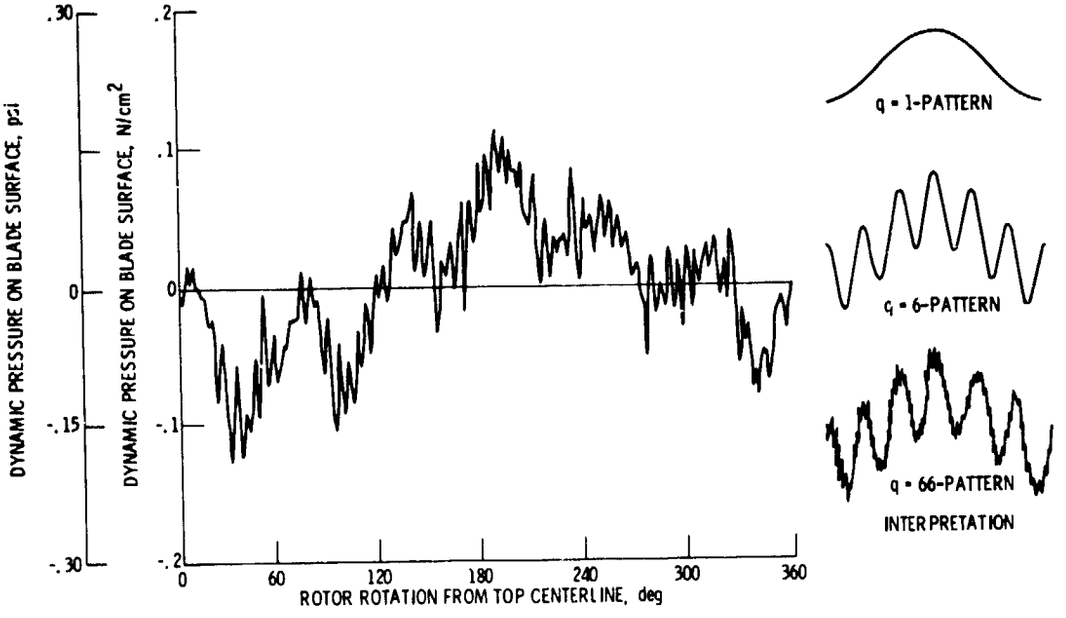

(a) PRESSURE WAVEFORM AVERAGED OVER 200 ROTOR REVOLUTIONS.

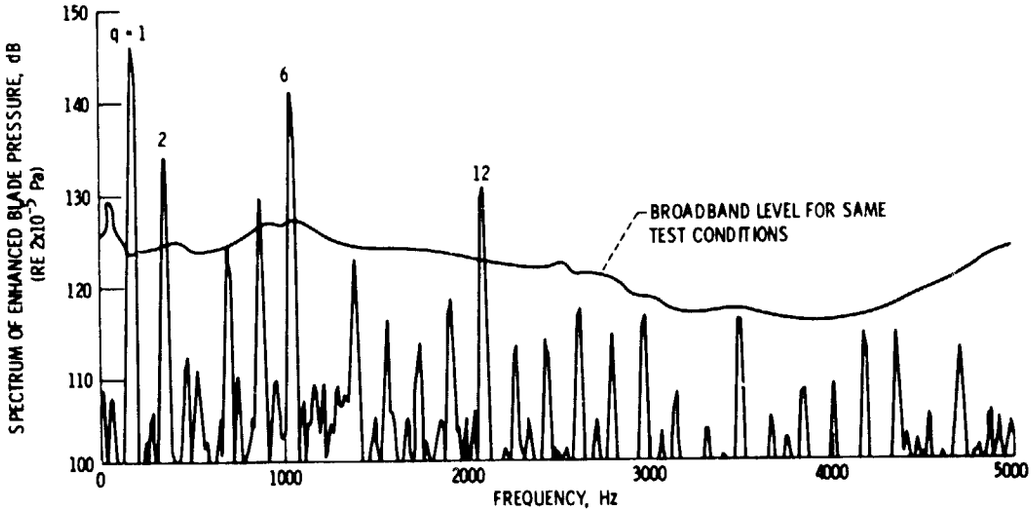

(b) SPECTRUM OF ENHANCED BLADE PRESSURE SIGNAL; ANALYZER BANDWIDTH 12.5 Hz.

Figure 8. - Signal enhanced waveform and spectrum (transducer B3, ICD 1, 10,500 rpm fan speed.)

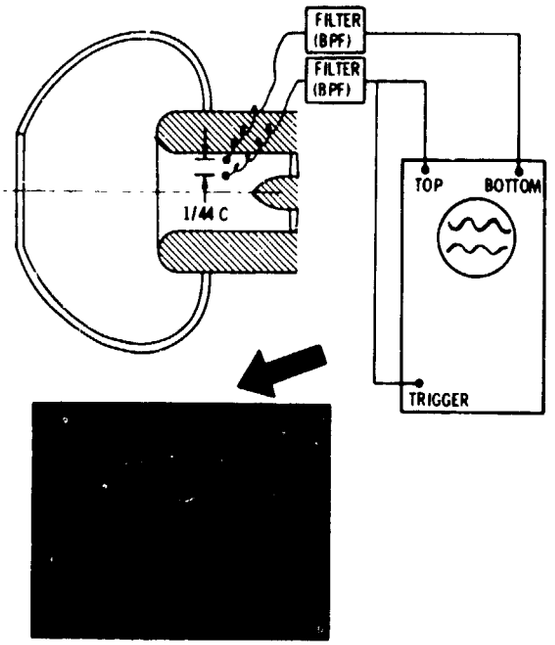

Figure 9. - Experiment to confirm m = 22 mode in duct.

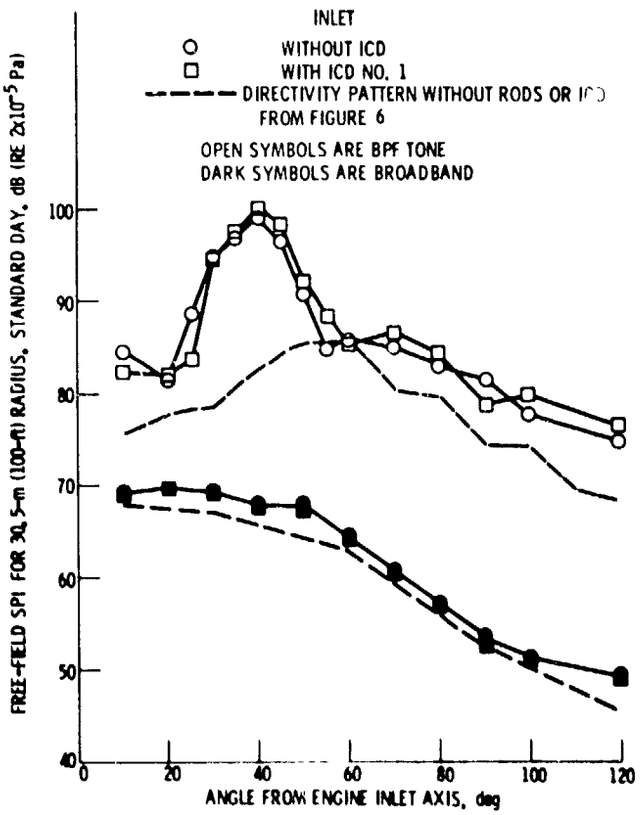

Figure 10. - Directivity patterns for acoustic transmission tests, 41 rods in inlet; corrected fan speed 10 500 rpm; analyzer bandwidth 25 Hz.

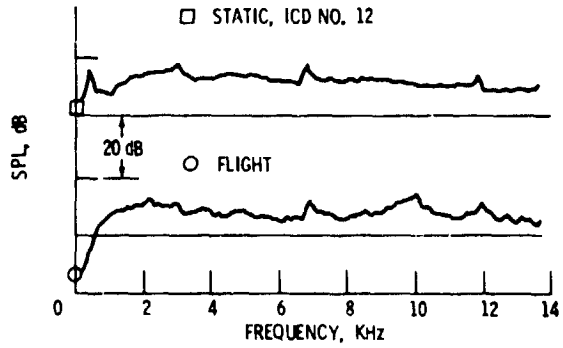

Figure 11. - Comparison of JT15D static and flight spectra, 10, 5000 rpm, 50° from inlet axis, static data use ICD No. 12.

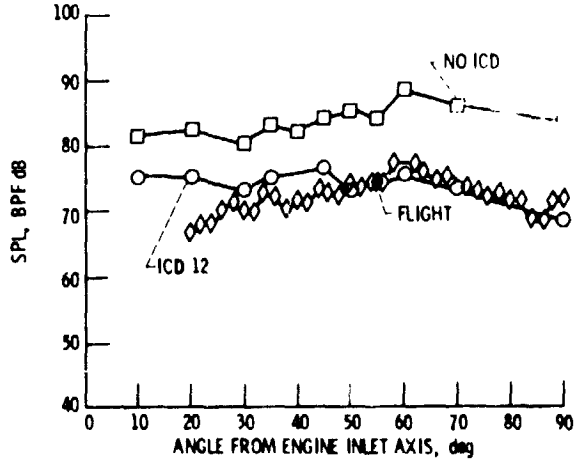

Figure 12. - Comparisons of BPF noise radiation patterns.

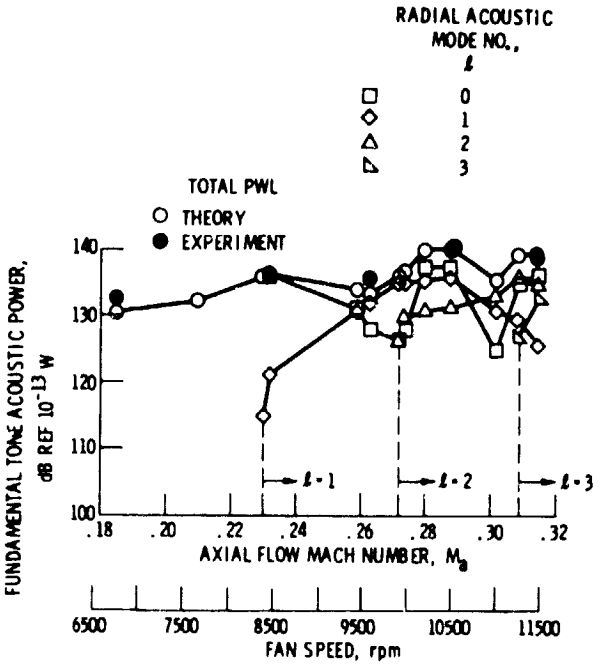

Figure 13. - Fan speed dependence of fundamental pure tone modal power generated by 41 rod wakes interacting with JT15D fan, upstream propagation.

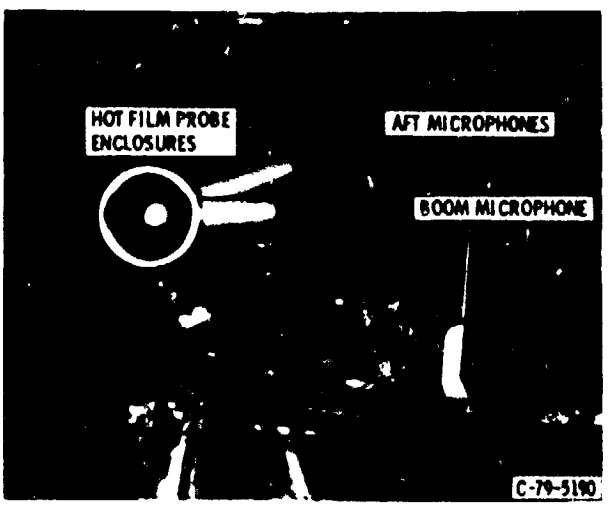

Figure 14. - Front view of fan in anechoic wind tunnel.

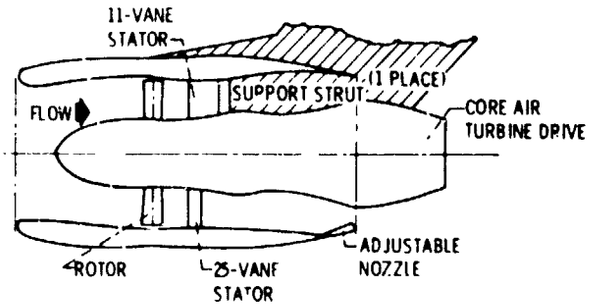

Figure 15. - Cross sectional view of fan stage. Stator is shown at intermediate spacing location.

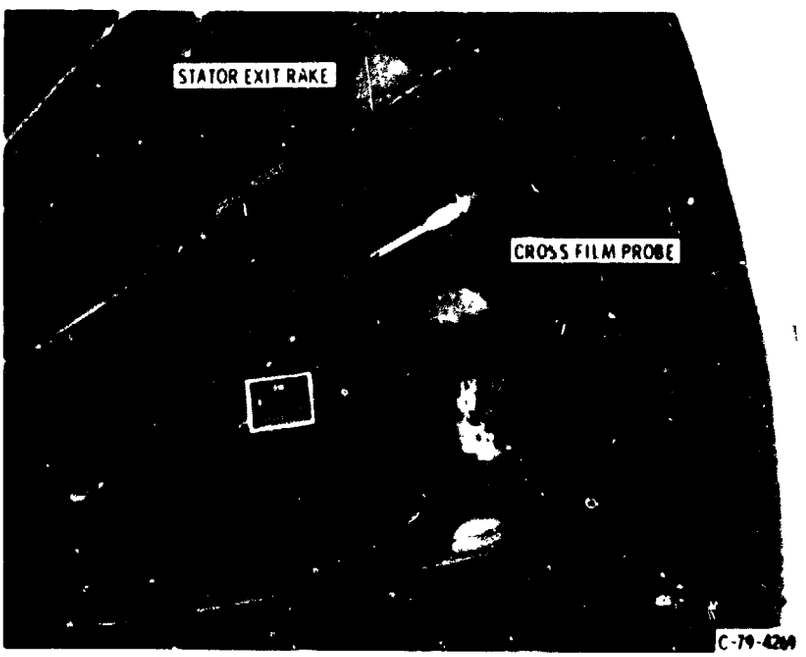

Figure 16. - Position of cross film relative to stator vanes.

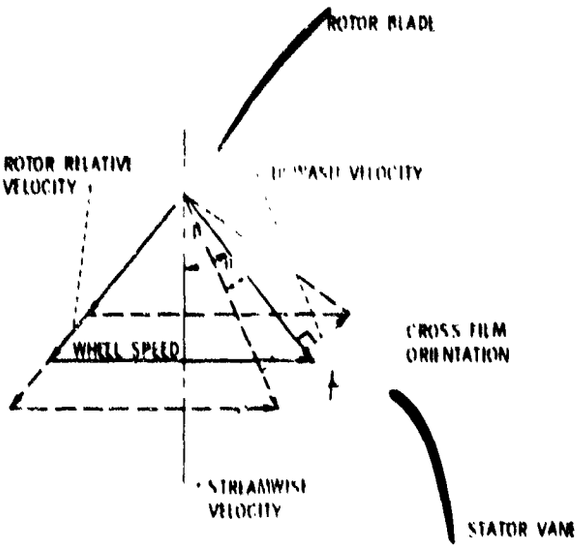

Figure 17. - Schematic of cross film orientation (β_1 = probe set angle, θ = fluctuating angle about β_1).

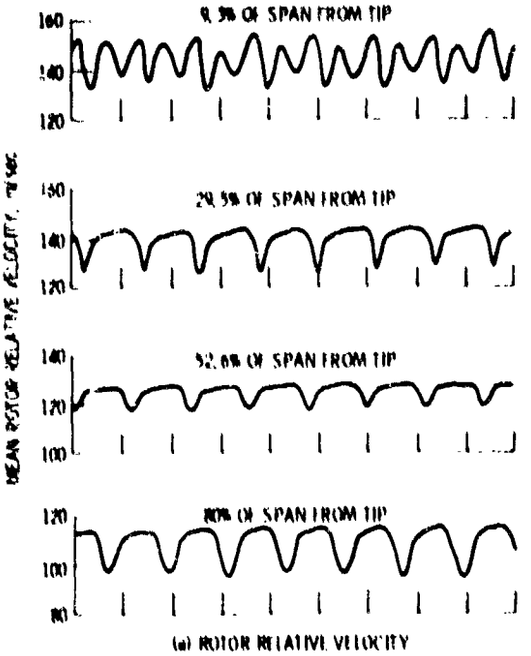

(a) ROTOR RELATIVE VELOCITY

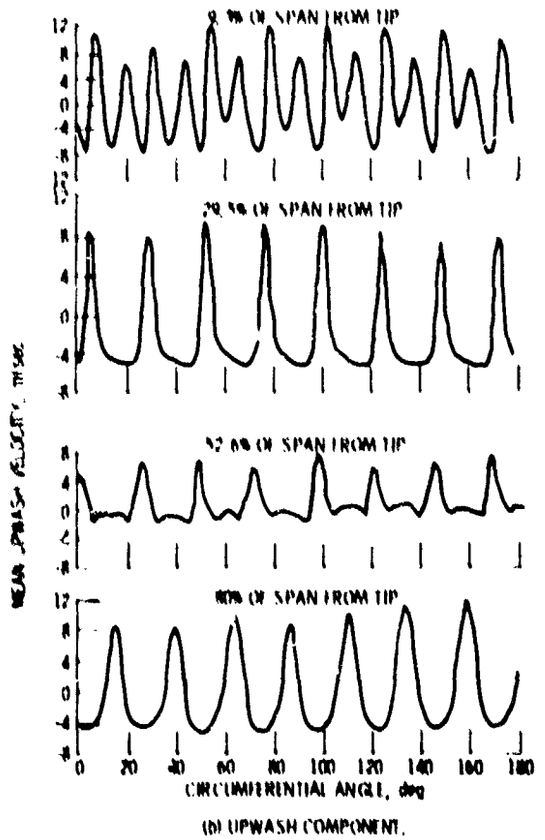

(b) UPWASH COMPONENT.

Figure 18. - Mean velocity across the duct at 80 percent of design rpm, U_{tunnel} = 41 m/sec, 1.29 c spacing.

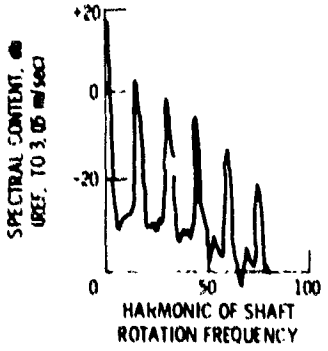

Figure 19. - Enhanced spectra of upwash velocity at 80 percent of design rpm, 1.25 chord spacing, 90 percent of span from the tip, U_{tunnel} = 41 m/sec.

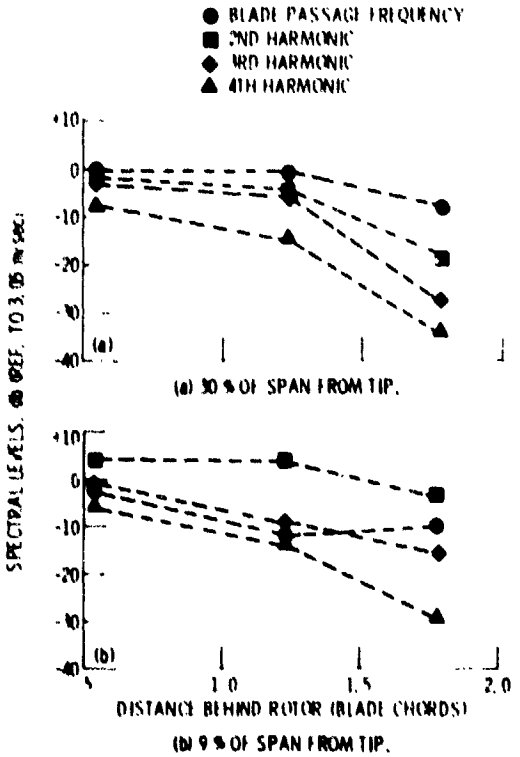

Figure 20. - Harmonic content of upwash wake component as a function of downstream distance, 80 % design speed. U_{tunnel} = 41 m/sec.

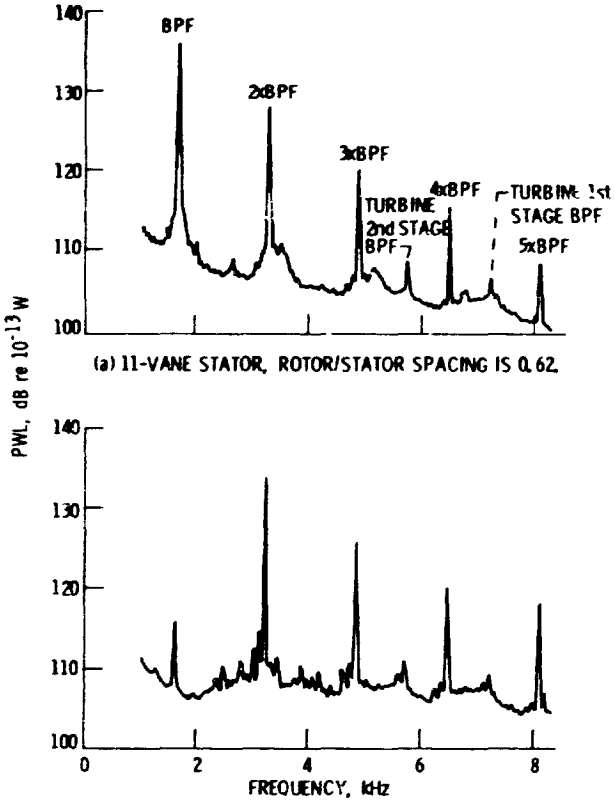

(a) 11-VANE STATOR, ROTOR/STATOR SPACING IS 0.62.

(b) 25-VANE STATOR, ROTOR/STATOR SPACING IS 0.74.

Figure 21. - Front quadrant PWL spectra, 80% design fan speed, 41 m/sec tunnel flow (20 Hz bandwidth).

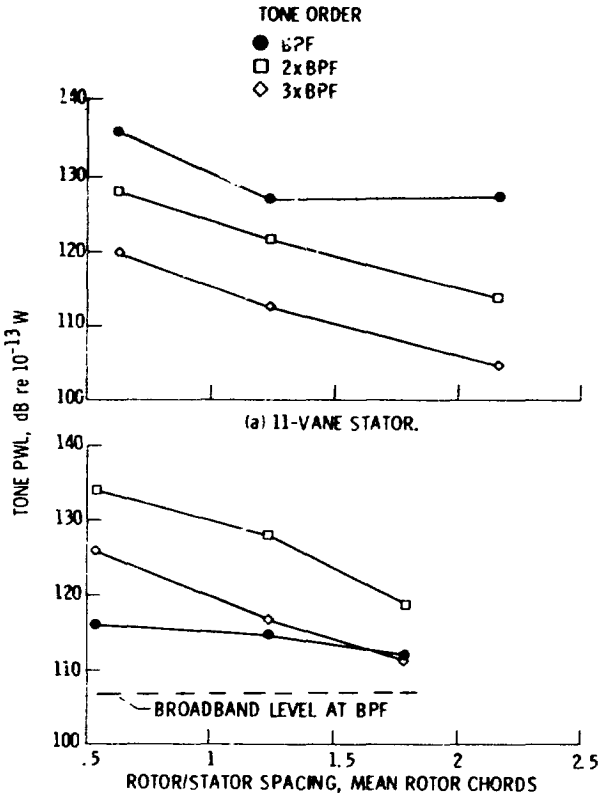

(a) 11-VANE STATOR.

(b) 25-VANE STATOR.

Figure 22. - Spacing effect on front quadrant tone, 80% design fan speed, 41 m/sec tunnel flow.

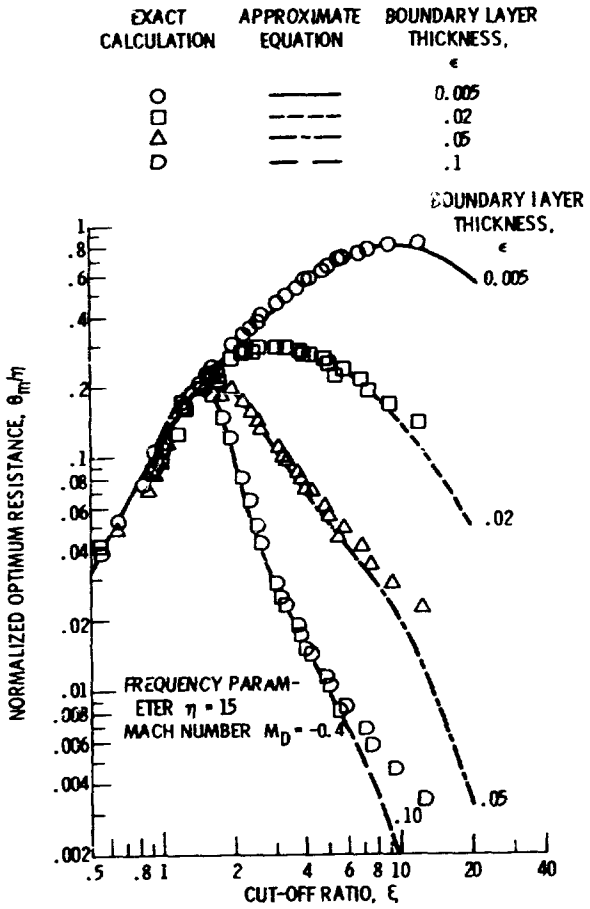

Figure 23. - Comparison of correlating equation with exact calculations of optimum resistance for variations in boundary layer thickness.

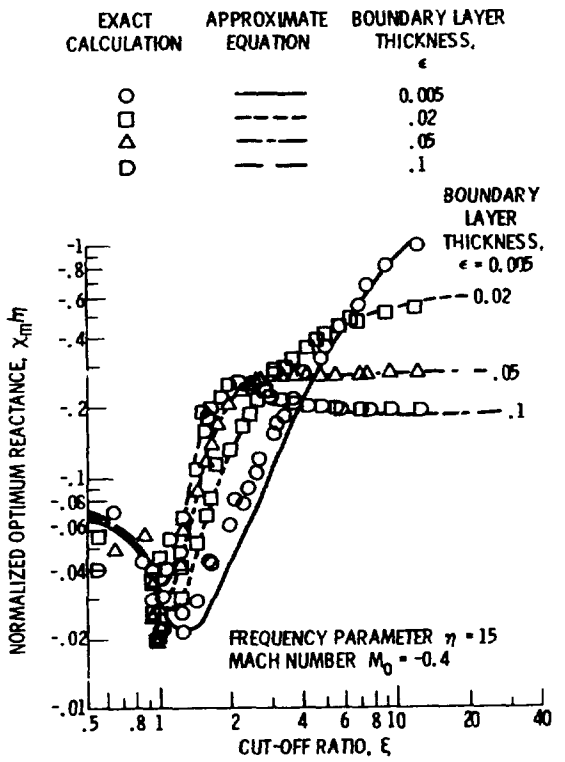

Figure 24. -Comparison of correlating equation with exact calculations of optimum reactance for variations in boundary layer thickness.

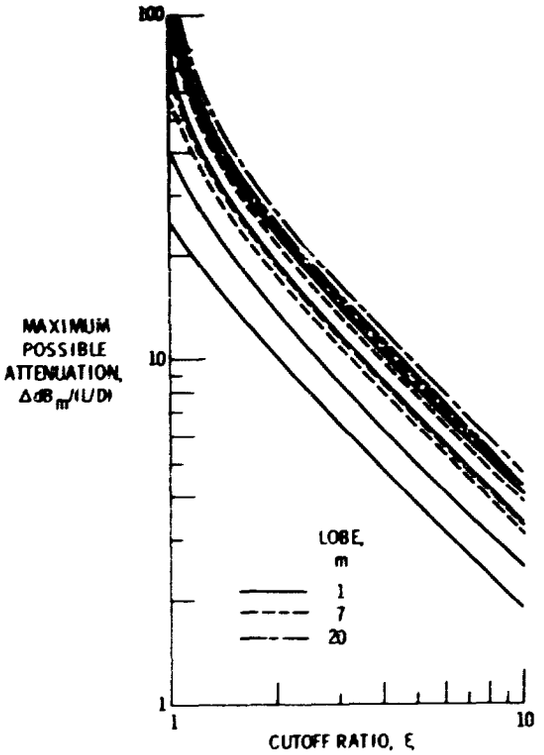

Figure 25. - Maximum possible attenuation as function of mode cutoff ratio. Zero Mach number.

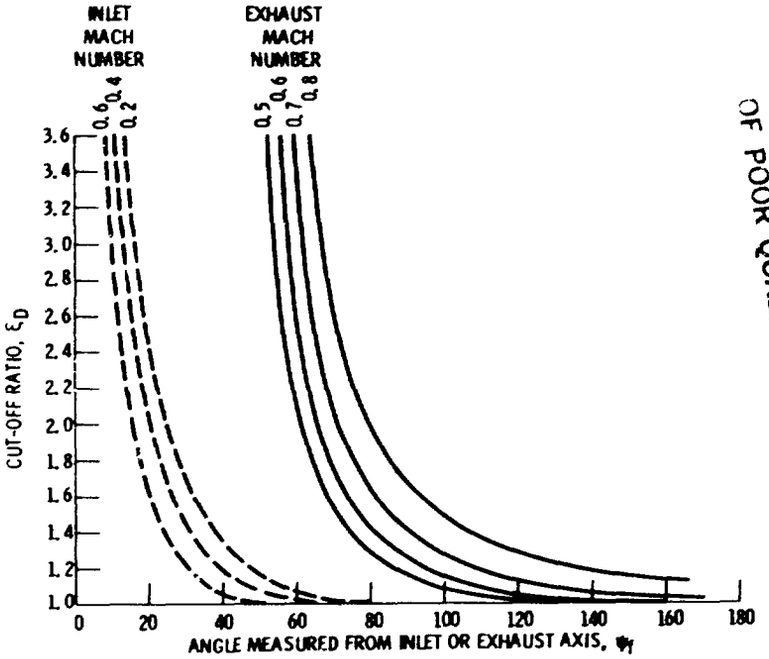

Figure 26. - Location of the peak of principal lobe of radiation as a function of mode cut-off ratio for inlets and aft ducts.

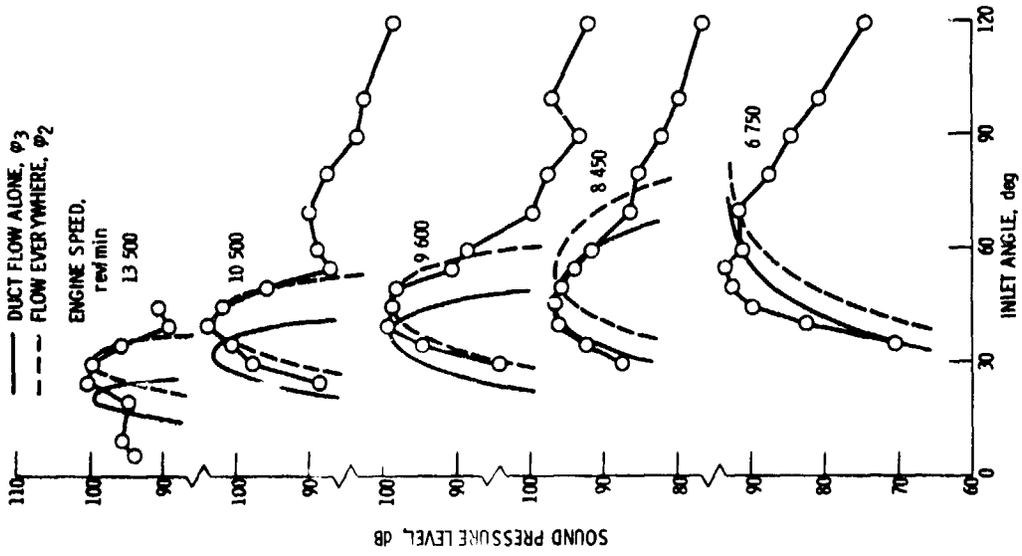

Figure 26. - Comparison of measured and predicted BPF tone directivities for 41-rod array.

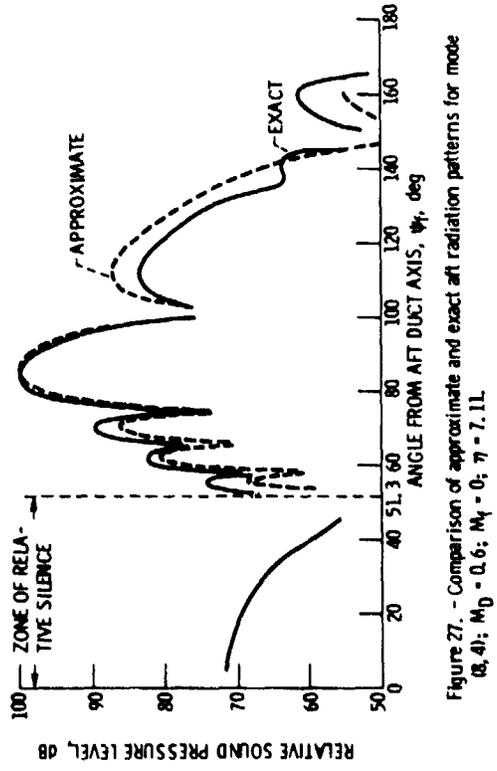

Figure 27. - Comparison of approximate and exact aft radiation patterns for mode (8, 4); $M_D = 0.6$; $M_t = 0$; $\eta = 7.11$.

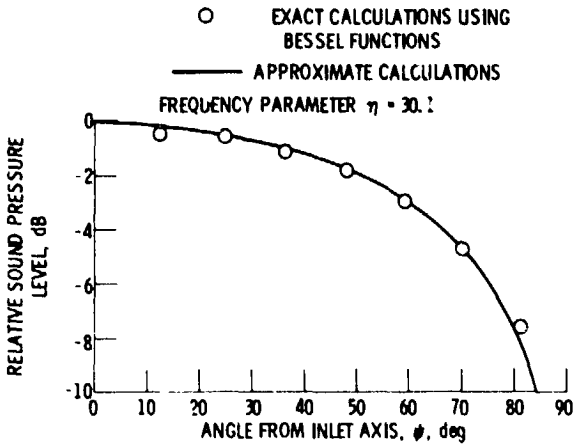

Figure 29. - Comparison of exact and approximate multimodal far-field directivity patterns for equal acoustic power per mode.

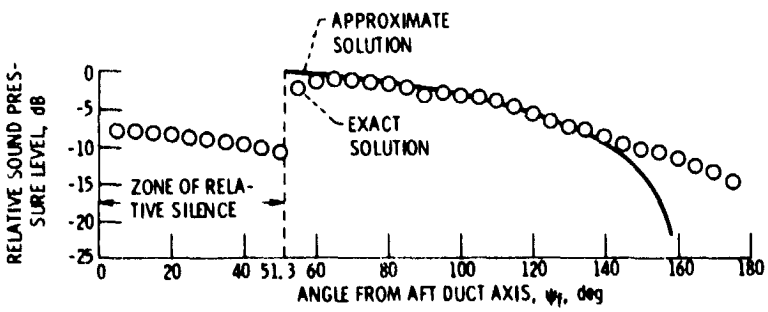

Figure 30. - Comparison of approximate and exact multimodal radiation patterns, 101 modes, equal power per mode, $M_D = 0.6$, $M_f = 0$, $\eta = 7.11$.

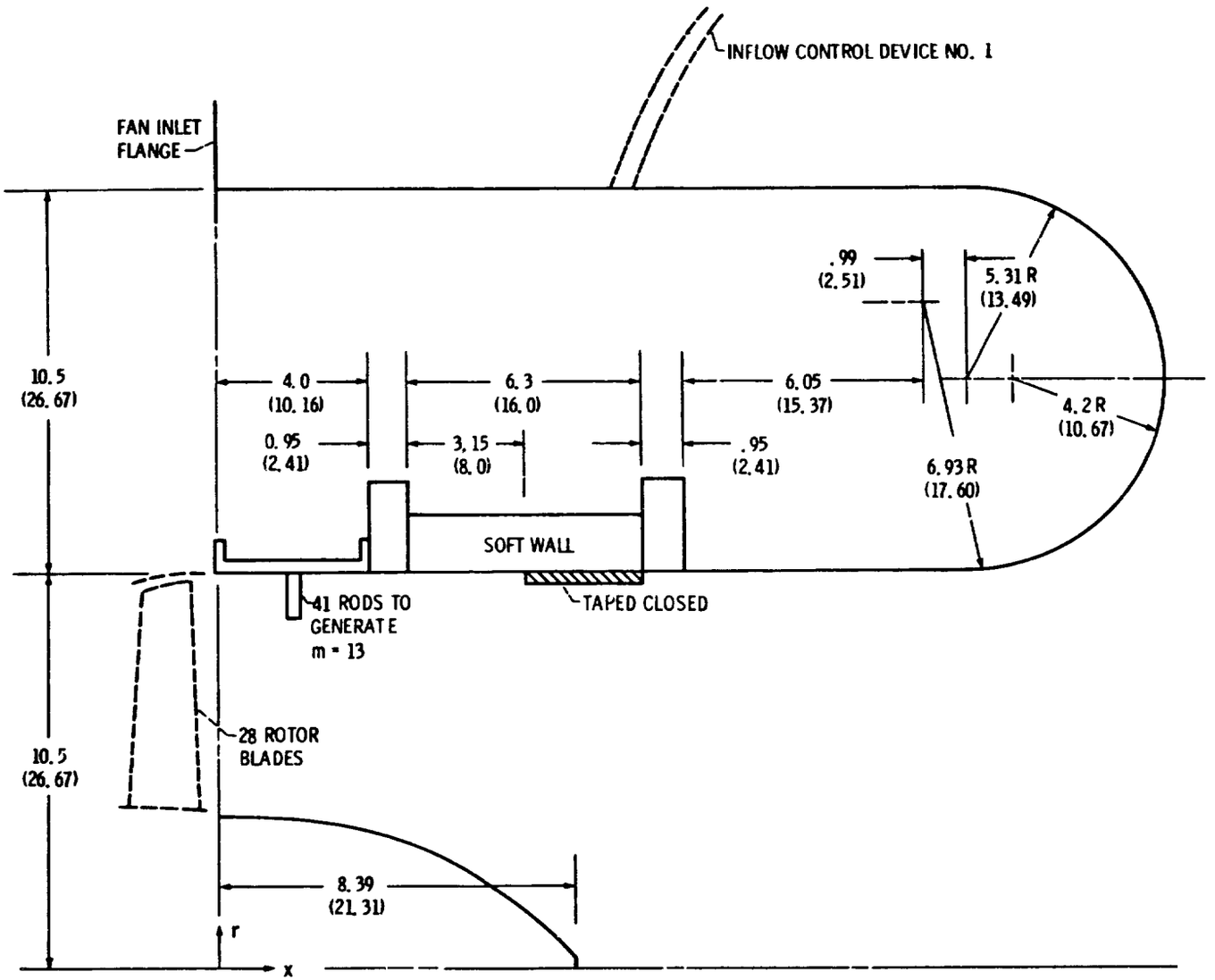

Figure 31. - Test configuration of JT15D engine inlet used for single mode SDOF suppressor experiments, dimensions in inches (cm).

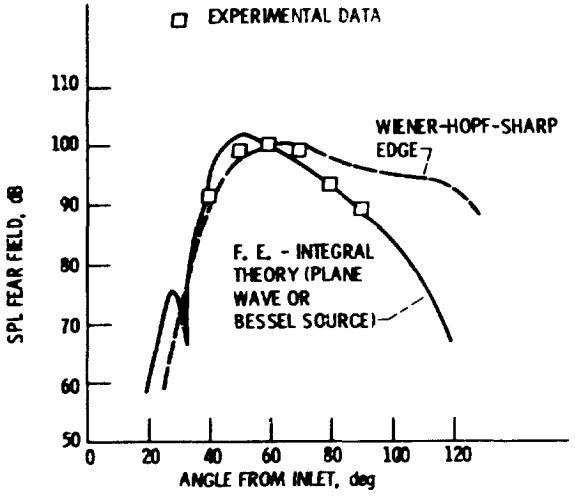

Figure 32. - Comparison of theory and experiment for narrow band tone directivity pattern at 3150 Hz and (13, 0) mode for hard wall configuration (theory and data normalized to 100 dB at 60 deg).

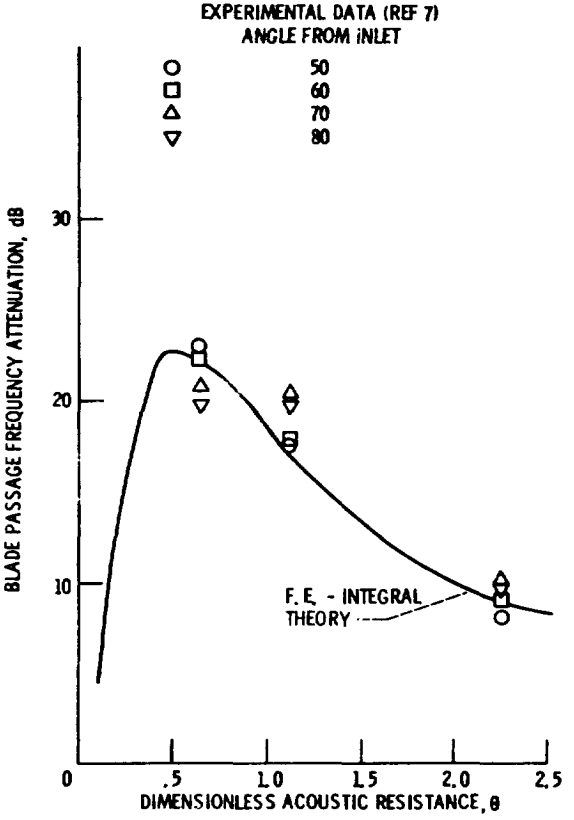

Figure 33. - Comparison of data with theoretical attenuation as a function of resistance for the (13, 0) mode at 3150 Hz (reactance $\chi = 0.5$) between 50-80 deg from inlet center line.